Response of the carbon cycle in an intermediate complexity model to the different climate configurations of the last 9 interglacials

Nathaelle Bouttes[1], Didier Swingedouw[1], Didier M. Roche[2,3], Maria F. Sanchez-Goni[1,4], Xavier Crosta[1]

[1] Univ. Bordeaux, EPOC, UMR 5805, F-33615 Pessac, France
[2] Laboratoire des Sciences du Climat et de l'Environnement, LSCE/IPSL, CEA-CNRS-UVSQ, Université Paris-Saclay, F-91191 Gif-sur-Yvette, France
[3] Earth and Climate Cluster, Faculty of Science, Vrije Universiteit Amsterdam, Amsterdam, The Netherlands
[4] EPHE, PSL Research University, F-33615 Pessac, France

Correspondence to: Nathaelle Bouttes (nathaelle.bouttes@lsce.ipsl.fr)

Abstract. Atmospheric CO_2 levels during interglacials prior to the Mid Bruhnes Event (MBE, ~430 ka BP) were around 40 ppm lower than after the MBE. The reasons for this difference remain unclear. A recent hypothesis proposed that changes in oceanic circulation, in response to different external forcings before and after the MBE, might have increased the ocean carbon storage in pre-MBE interglacials, thus lowering atmospheric CO_2. Nevertheless, no quantitative estimate of this hypothesis has been produced up to now. Here we use an intermediate complexity model including the carbon cycle to evaluate the response of the carbon reservoirs in the atmosphere, ocean and land in response to the changes of orbital forcings, ice sheet configurations and atmospheric CO_2 concentrations over the nine last interglacials. We show that the ocean takes up more carbon during pre-MBE interglacials in agreement with data, but the impact on atmospheric CO_2 is limited to a few ppm. Terrestrial biosphere is simulated to be less developed in pre-MBE interglacials, which reduces the storage of carbon on land and increases atmospheric CO_2. Accounting for different simulated ice sheet extents modifies the vegetation cover and temperature, and thus the carbon reservoir distribution. Overall, atmospheric CO_2 levels are lower during these pre-MBE simulated interglacials including all these effects, but the magnitude is still far too small. These results suggest a possible mis-representation of some key processes in the model, such as the magnitude of ocean circulation changes, or the lack of crucial mechanisms or internal feedbacks, such as those related to permafrost, to fully account for the lower atmospheric CO_2 concentrations during pre-MBE interglacials.

1 Introduction

Ice core data have shown that atmospheric CO_2 concentration has been different during interglacials of the last 800,000 years (Luthi et al., 2008; Bereiter et al., 2015). Older interglacials before the Mid-Bruhnes Event (MBE) around 430 ka BP, i.e. Marine Isotope Stage (MIS) 13, 15, 17 and 19, are characterised by relatively lower atmospheric CO_2, around 240 ppm, compared to more recent interglacials, i.e. MIS 1, 5, 7, 9 and 11, which have a higher CO_2 level of around 280 ppm (Figure 1a).

Proxy data such as the marine benthic foraminifera $\delta^{18}O$ stack record, embedding both deep-sea temperature and ice-sheet volume (Lisiecki and Raymo, 2005), indicate that older interglacials (pre-MBE) experienced a colder climate than the more recent ones (post-MBE). This tendency is also supported by individual $\delta^{18}O$ and sea-surface temperature (SST, derived from Mg/Ca paleothermometry, alkenones or foraminifera assemblages) records from marine sediment cores (Lang and Wolff, 2011; Past Interglacials Working Group of PAGES, 2016), although some individual sub-stages such as MIS 7c and 7e were colder than the post-MBE mean interglacial climate.

To explain the different climates of interglacials before and after the MBE, modelling studies have shown that it is necessary to include the change of atmospheric CO_2 (Yin and Berger, 2010; 2012). Indeed, these numerical simulations with an intermediate complexity model have demonstrated that differences in Earth's orbital configuration, and hence seasonal and spatial distribution of insolation, cannot explain alone the colder climate recorded during pre-MBE interglacials, whereby lower atmospheric CO_2 concentration is also necessary to simulate colder climate (Yin and Berger, 2010; 2012). However, the reasons for the lower CO_2 values remain elusive and very few modelling exercises have tackled the issue of different CO_2 levels during interglacials before and after the MBE. Köhler and Fischer (2006) have produced transient simulations of the last 740,000 years using the BICYCLE box model. They used several paleoclimatic records such as ocean temperature, sea ice, sea level, ocean circulation, marine biota, terrestrial biosphere and $CaCO_3$ chemistry to force forward their model. They run a set of simulations prescribing only one forcing at a time and another with all forcings excluding one at a time, which allows them to analyse which forcings are the most important. In their simulations, they have shown that the lower CO_2 values during pre-MBE are mainly explained by the prescribed lower Southern Ocean (SO) sea surface temperature and weaker Atlantic meridional overturning circulation (low North Atlantic Deep Water formation and SO vertical mixing) compared to post-MBE interglacials. Using an intermediate complexity model, Yin (2013) conversely simulated vigorous bottom water formation and stronger ventilation in the Southern Ocean during pre-MBE interglacials and suggested this could increase deep oceanic carbon storage and lower atmospheric CO_2. However, this effect on the ocean carbon reservoir and atmospheric CO_2 has not been evaluated yet in a climate model including a carbon cycle representation.

Changes in surface temperature also modify the partition of the carbon cycle: in the ocean, colder SST increases the solubility of CO_2, increasing its potential uptake from the atmosphere during pre-MBE interglacials. In contrast, on land a colder climate might yield a decrease in biomass reducing CO_2 uptake *via* lower continental carbon storage. Because the ice

sheets in the North Hemisphere are different during the interglacials in response to the different values of CO_2 and orbital configurations (Ganopolski and Calov, 2011), they might also have an impact on the carbon cycle, for example by modifying the terrestrial biosphere extent.

Here, we test the impact of the different orbital configurations of the last nine interglacials on the carbon cycle. For this purpose, we use a coupled carbon-climate model to evaluate the changes of carbon storage in the ocean and in the terrestrial biosphere, as well as the impact of different North Hemisphere ice sheet volumes.

2 Methods

We use the iLOVECLIM climate model of intermediate complexity, which is a new development branch (code fork) of the LOVECLIM model in its version 1.2 (Goosse et al., 2010). iLOVECLIM has an atmosphere module (ECBILT) with a T21 spectral grid truncation (~5.6° in latitude/longitude in the physical space) and 3 vertical layers. The ocean component (CLIO) has a horizontal resolution of 3° by 3° and 20 vertical levels. The evolution of the terrestrial biosphere, i.e. the proportion of desert, grasses and tree cover, is computed by the VECODE model (Brovkin et al., 1997). It includes a carbon cycle module on land and in the ocean (Bouttes et al., 2015). iLOVECLIM is an evolution from the LOVECLIM model used in previous model studies of the last nine interglacials focused on climate (Yin and Berger, 2010; 2012; Yin, 2013). It has the same atmospheric and oceanic modules, but includes a different carbon cycle representation in the ocean (Bouttes et al., 2015). We have chosen the same dates for the nine orbital configurations as in Yin and Berger (2010; 2012) and Yin (2013), *i.e*. the maximum of insolation preceding the $\delta^{18}O$ peak values (Table 1, Figure 1b and c). Contrary to most simulations from these studies, we also use the CO_2 values (as well as CH_4 and N_2O) at the same dates as for the orbital configurations (and not at the CO_2 peak), but as stated in Yin and Berger (2012), this may not affect the main results concerning the simulated climatic changes.

MIS	**Date of $\delta^{18}O$ peak (ka BP)**	**Date for orbital configuration and CO_2 (ka BP)**	**CO_2 values from data (ppm)**	**Sea level changes (m) corresponding to the ice sheet configurations**
1	6	12	243.2	13.8
5.5	123	127	268.64	-0.8
7.5	239	242	269.23	5.6
9.3	329	334	280.32	-0.9
11.3	405	409	282.29	-0.8

13.13	501	506	235.92	13.1
15.1	575	579	249.36	2.3
17	696	693	234.38	-0.4
19	780	788	242.73	10.8

Table 1 Dates of orbital parameters and CO_2 used for the simulations (Luthi et al., 2008), and sea level anomalies as compared to present-day conditions (m) corresponding to the prescribed ice sheets (Ganopolski and Calov, 2011).

In the model, we separate the atmospheric CO_2 concentration into two distinct variables depending on its physical and chemical impact. The first one is used in the radiative scheme of the atmosphere, for which we prescribe in all the described simulations the CO_2 from measured values (Lüthi et al., 2008; Figure 1a). Another atmospheric CO_2 is computed interactively in the model, as a result of the balance of the carbon fluxes between the different carbon sub-components (atmosphere, ocean and terrestrial biosphere). We make this choice of keeping the two separated to ensure that the climate simulated by the model is coherent with past measured atmospheric CO_2. In other words, we consider the atmospheric CO_2 concentration as an imposed external forcing, while within the carbon cycle the atmospheric CO_2 concentration is allowed to vary, but does not impact the atmospheric radiative forcing. By doing this, we limit the number of degrees of freedom in our climate carbon system, which notably allows to avoid the complication arising from simulating a different climate when the climate-carbon is fully coupled.

The simulations performed are snapshots, run with constant orbital and atmospheric CO_2 concentration forcing and integrated over 3000 years allowing the ocean to reach a quasi-equilibrium. All simulations start from the pre-industrial control one, and the average of the last 100 years is used to analyse the results.

Our strategy is to evaluate the impact of the different climate and carbon compartments to set the atmospheric CO_2 concentration. For this purpose, we consider three series of simulations, which have all been run for the nine interglacials (Table 2). The first series (OC "Ocean Carbon") has fixed ice sheets set to the observed pre-industrial ones and fixed terrestrial biosphere set to the simulated pre-industrial one. This first set of simulations thus provides the response of the ocean alone to the different orbital parameters and CO_2 levels of the nine interglacials. The second series (OVC "Ocean Vegetation Carbon") has still fixed ice sheets, but includes an interactive terrestrial biosphere, computed by the model. It gives the response of both the ocean and land vegetation reservoirs to the different orbital parameters and CO_2 as well as their interactions for setting the atmospheric CO_2 concentration. Finally, the third series (OVIC "Ocean Vegetation Ice sheet Carbon") has different prescribed ice sheets in the North Hemisphere for the nine interglacials. The ice sheet distribution change is based on modelling results, given that the uncertainty from data is very large for the interglacials of the last 800,000 years, especially the oldest ones. The prescribed ice sheet distributions are thus taken from an ice sheet simulation

of the last 800,000 years (Ganopolski and Calov, 2011) using the intermediate complexity model CLIMBER-2 (Petoukhov et al., 2000; Ganopolski et al., 2001; Brovkin et al., 2002), including a 3-D polythermal ice sheet model (Greve, 1997). This ice sheet model is coupled to the climate component via surface energy and mass balance interface (Calov et al., 2005), which accounts for the effect of aeolian dust deposition on snow albedo. The ice sheet distribution is chosen 2,000 years after the chosen interglacial date to account for the long timescale of the ice sheet response during a deglaciation and ensure that the ice sheet corresponds to an interglacial configuration. The ice sheet elevations for the nine interglacial simulations are shown on Figure 2 and the corresponding sea level change in Table 1. The terrestrial biosphere is also interactive in this OVIC series of simulations. This last set of simulations thus adds the effect of having different ice sheets in the North Hemisphere for the carbon cycle variations.

Name of the series	Components impacting the carbon cycle		
	Ocean	Vegetation	Different interglacial ice sheets
OC	✓	✗	✗
OVC	✓	✓	✗
OVIC	✓	✓	✓

Table 2. Summary of the three series of simulations.

3 Results and discussion

3.1 Role of the ocean (OC simulations)

Similar to previous numerical studies of the interglacials with the LOVECLIM model (Yin and Berger, 2010; 2012), the changes in orbital configuration and atmospheric CO_2 altered SSTs and oceanic circulation for each interglacial simulation of the OC series. All simulations have warmer SSTs than the control pre-industrial in the North Hemisphere high latitudes (Figure 3). Except for MIS1, the SSTs in the post-MBE simulations (corresponding to MIS 5, 7, 9 and 11) are also warmer than in the pre-industrial control in large areas in the North Hemisphere mid-latitudes. In the MIS 5, 9 and 11 simulations the SSTs are slightly warmer in the Southern Ocean. In the pre-MBE simulations (MIS 13, 15, 17 and 19), the ocean is mainly

colder than the pre-industrial, especially in the Southern Hemisphere. To compare the pre-MBE to post-MBE simulations, we built a composite (average) for each period (pre- and post-MBE). We have excluded MIS 1 from the post-MBE composite, for which the date chosen corresponds to a CO_2 much lower than the other post-MBE interglacials. We thus consider MIS 5, 7, 9 and 11 in the post-MBE composite and MIS 13, 15, 17 and 19 in the pre-MBE composite. The difference between the pre- and post-MBE composites shows colder SSTs in the pre-MBE interglacial simulations compared to the post-MBE simulations, especially in the Southern Ocean (Figure 4a). The difference in global mean simulated SST is -0.30 °C, reaching up to -0.36°C in the North Atlantic (between 30°N and 65°N) and -0.43°C in the Southern Ocean (south of 54°S). This is in general agreement with SST data, which indicate colder SST in the pre-MBE interglacial oceans, especially in the Southern Ocean (Table 3 and figure 4a), although the comparison is limited by the lack of SST records across the MBE.

latitude (°)	**Longitude (°)**	**Site**	**MIS 5e**	**MIS 7e**	**MIS 9e**	**MIS 11c**	**MIS 13a**	**MIS 15a**	**MIS 17c**	**MIS 19c**	**post-MBE**	**pre-MBE**	**Difference pre-post MBE**
57.51	-15.85	ODP 982	16.2	14.5	15.8	15	13.7	14.1	14.2	14.1	15.4	14.0	-1.35
56.04	-23.23	DSDP 552s	15.1	14.7	14.2	16.4	12.4	14.7	18.3	14.7	15.1	15.0	-0.08
41.01	-126.43	ODP 1020	14.1	11.7	12.8	14	10.2	12.5	13.6	12.1	13.2	12.1	-1.05
41.00	-32.96	DSDP 607s	25.1	20.5	23.6	26.8	22.3	20.3	25.2	24	24	23.0	-1.05
32.28	-1148.40	ODP 1012	19.5	17.7	19.7	19.1	17.5	18.3	19.3	18	19	18.3	-0.73
19.46	116.27	ODP 1146	27.3	26.3	27.3	26.8	26.1	26.3	26.9	26.2	27.0	26.4	-0.55
16.62	59.80	ODP 722	27.7	27.3	27.5	27.5	27	27.1	27.2	27.2	27.5	27.1	-0.38
9.36	113.29	ODP 1143	28.8	27.8	28.6	28.3	28.4	28.1	28.6	28.2	28.4	28.3	-0.05
2.04	141.76	MD97-2140	29.5	28.6	29	29.5	28.6	28.4	29.3	28.9	29.2	28.8	-0.35
0.32	159.36	ODP 806B	29.6	29.2	28.8	30.2	28.2	29.4	29	29.4	29.5	29	-0.45
-3.10	-90.82	ODP 846	25.1	24	23.8	24	23.6	23.7	23.7	23.7	24.2	23.7	-0.55

-41.79	-171.50	ODP 1123	17.7	19	19.6	19.3	17.8	18.8	18	17.9	18.9	18.1	-0.78
-42.91	8.9	ODP 1090	17.1	10.2	14.7	13.9	10.2	11.7	11.1	10.4	14.0	10.9	-3.125
-43.45	167.9	MD06-2986	18	16.5	16.6	18.1	15.5	16.2	16.3	15.8	17.3	16.0	-1.35
-45.52	174.95	DSDP594	18.3	7.1	9.5	17.5	10	11.7	12.1	9.7	13.1	10.9	-2.23

Table 3. SST data (in °C) from Past Interglacials Working Group of PAGES (2016) and shown on Figures 4a, b and 14.

Compared to the pre-industrial period, the ventilation of the Southern Ocean is increased in all simulations (Figure 5). The formation of AABW as well as the wind driven meridional cell between 40 and 60°S (so called Deacon cell) are both stronger. On average, the maximum of the Deacon cell is increased by 7% between pre- and post-MBE simulations, while AABW is increased by 18% (Figure 4c). The meridional overturning circulation is also slightly increased by 6% and deepened in the Atlantic Ocean. All these results concerning oceanic circulation changes are very similar to those of Yin et al. (2013), allowing to test their hypothesis on the impact of these changes on ocean carbon uptake and atmospheric CO_2 concentrations.

The changes in global ocean circulation and SST modify the carbon storage in the ocean. The colder SST, which increases dilution of CO_2 at the ocean surface, associated with stronger ventilation in the pre-MBE simulations yield a larger carbon uptake by the ocean. Such processes result in higher dissolved inorganic carbon (DIC) concentrations in the Southern Ocean, as well as higher DIC concentration in the upper ocean (first 2 km of the ocean) (Figure 4e), reflecting the average increase of 4.7 GtC in pre-MBE simulations. On the opposite, the DIC slightly decreases in the deeper ocean, which may be due to the increased ventilation of NADW bringing more carbon back from the deep ocean to the surface.

The stronger uptake of carbon by the ocean leads to a decrease in atmospheric CO_2 concentration during the pre-MBE interglacials compared to the post-MBE ones (Figure 6), in agreement with CO_2 data as shown by the very good correlation between the measured and simulated values ($r=0.91$, $p<0.01$, Fig. 6). However, the difference in magnitude between pre- and post-MBE values is only a few ppm in the simulations. Thus, even though simulations qualitatively reproduce the geological CO_2 trend, with lower values during the pre-MBE than the post-MBE interglacials, the magnitude of the difference is much lower in the simulation (~1-5 ppm) than in the data (~30-40 ppm). In fact, the slope of the linear regression between simulated atmospheric CO_2 concentration and observed ones is 0.07, indicative of a ~14 times underestimation by the simulations.

Hence the ocean carbon uptake in the simulations is not sufficient to drive a significant lowering of atmospheric CO_2. Either the change in global ocean circulation and SST should be larger, or another mechanism and feedbacks need to be taken into account to modify the biological or physical carbon uptake and amplify the initial change. Since the representation of bottom water formation in the Southern Ocean is biased in the model with an over-representation of open ocean convection, as is

also the case for many more complex General Circulation Models (GCMs) (Heuzé et al., 2013), it is possible that this hinders simulating the full range of carbon storage due to ocean circulation changes, as it is suspected for colder periods such as the Last Glacial Maximum (around 21,000 years ago) (Fischer et al., 2010).

3.2 Role of land vegetation and soils (OVC simulations)

In the first series of simulations, solely the ocean was allowed to respond to the different external forcings while land vegetation and soils were fixed to their pre-industrial distribution. To account for changes in land vegetation and soils on the carbon cycle, a second series of simulations (OVC) was conducted with an interactive terrestrial biosphere module on top of the ocean's one (Table 2).

Compared to the pre-industrial control simulation, more trees develop in North Africa and the southern part of Eurasia in these interglacial simulations, while the tree cover is reduced in central North America and some regions in the northern part of Eurasia (Figure 7). When compared to OC simulations with fixed vegetation, the OVC simulations demonstrate a surface ocean warming almost everywhere except in the North Atlantic for some interglacials (Figure 8). In response to the global warmer surface ocean, the stratification in the convection region in the North Atlantic increases (*e.g.* Swingedouw et al., 2007a) leading to a slowdown of the Atlantic Meridional Oceanic Circulation (AMOC), especially for MIS 1, 5 7, 9 and 15 (Figure 9).

For the carbon cycle, the activation of the terrestrial module results in more carbon stored in land vegetation and soils for all interglacial simulations (Figure 10b) since the vegetation cover increases compared to the control because of the warmer climate. This tends to lower atmospheric CO_2 concentration, hence the pCO_2 difference at the air-sea interface, leading to an outgassing of carbon from the ocean to the atmosphere, which ultimately decreases the storage of carbon in the ocean. The ocean carbon storage is also diminished compared to the series of simulations with fixed vegetation due to the warmer ocean temperature, which reduces the CO_2 solubility in water. The increase of carbon storage in the terrestrial biosphere is generally larger than the loss of carbon from the ocean so that the carbon content of the atmosphere is also diminished in these simulations compared to the fixed vegetation simulations, and atmospheric CO_2 is slightly lower or not changed (Figure 11a).

In terms of difference between pre- and post-MBE interglacial simulations, we find less vegetation cover in most areas (except in North Africa and parts of south Eurasia) and consequently less carbon stored (-48 GtC) in land vegetation and soils in the pre-MBE simulations compared to post-MBE simulations (Figure 12). This effect tends to increase atmospheric CO_2 on average in pre-MBE interglacial simulations.

For the ocean, the differences between pre- and post-MBE simulations are similar to the ones for the simulations with fixed vegetation (OC). On average, the SST is lower in the pre-MBE simulations compared to post-MBE simulations (-0.28°C globally, -0.31°C in the North Atlantic and -0.44°C in the Southern Ocean) except in a small area in the North Atlantic (Figure 4b) and the ventilation is increased in the pre-MBE simulations (Figure 4d). Hence the ocean can store more carbon

in the pre-MBE simulations than the post-MBE simulations with an average increase of carbon storage in the pre-MBE ocean of 43 GtC compared to the post-MBE ocean. Similarly, the DIC concentration is higher in pre-MBE simulations, especially in the upper ocean and deep Southern Ocean, as in the previous series of simulations with fixed vegetation (Figure 4f).

As the diminution in land carbon storage is larger than the increase in ocean carbon storage, more carbon is conserved in the atmosphere resulting in higher CO_2 on average for the pre-MBE simulations than the post-MBE simulations (Figure 11b). There is thus a qualitative disagreement (negative correlation of -0.33 (p=0.38) between simulated and observed atmospheric CO_2 for the interglacials considered) with the observations.

Nevertheless, it should be noted that permafrost (frozen soil) was not taken into account in these simulations. If there was more permafrost during the colder pre-MBE interglacials, it could store more carbon on land and counteract the loss of carbon due to the reduction of vegetation cover and production (Crichton et al., 2016).

Comparison with pollen data (Table 4) indicates that the model is in qualitative agreement with reconstructed tree cover change in South America where the tree cover was smaller on average in pre-MBE than in post-MBE interglacials (Figure 12a). In southern Europe, the tree fraction data indicate that on average slightly more tree cover prevailed during pre-MBE than during post-MBE interglacials, also in agreement with simulations, although the variability in the data among interglacials is large.

		SW Iberian margin (MD95-2042, MD01-2443, IODP U1385) Tree cover = Mediterranean Forest pollen %		**Tenaghi-Phillipon Tree cover = Temperate Forest pollen %**		**Funza Arboreal pollen%-Quercus %**	
		Interglacial values	Average	Interaglacial values	average	Interglacial values	average
Post-MBE	**MIS5e**	68	53.0	96	95.9	86	76.7
	MIS7e	42		92.4		75	
	MIS9c	54		95.5		73	
	MIS11c	48		99.5		73	
Pre-MBE	**MIS13a**	48	57	95.8	89.5	73	71.2
	MIS15a	54		96.9		65	
	MIS17c	78		82.2		78	

	MIS19c	47		83.3		69	
Difference Pre-MBE – post-MBE			4		-6.4		-5.5

Table 4: Tree cover (%) reconstructed from pollen data in three sites. SW Iberian margin: MIS 5 (MD95-2042, Sanchez Goñi et al., 1999), MIS 7 (MD01-2443, Roucoux et al., 2006), MIS 9, 13, 15, 17 (IODP 1385, unpublished data), MIS11 (U1385, Oliveira et al., 2016), MIS 19 (U1385, Sanchez Goñi et al., 2016); Tenaghi-Phillipon, Greece (Past Interglacials Working Group of PAGES, 2016); and Funza, Colombia (Past Interglacials Working Group of PAGES, 2016).

3.3 Impact of different ice sheets (OVIC simulations)

The last series of simulations (OVIC) has the same design as OVC but also takes into account possible differences in ice sheet distribution in the North Hemisphere based on numerical simulations (Ganopolski and Calov, 2011). The simulated ice sheet distributions used for our interglacial simulations mainly differ in North America. On average, the North American ice sheet is more extended in the pre-MBE interglacials compared to the post-MBE interglacials (Figure 13).

The change of ice sheet extent has a large regional impact on vegetation cover, which is reduced where the ice sheet extends more. On average, it results in a reduction of vegetation in North America in the pre-MBE interglacials, when the ice sheet is more extended, compared to the post-MBE interglacials (Figure 12b, d).

The increase in ice sheet extent and diminution of vegetation cover for pre-MBE simulations has two main impacts for the carbon cycle: (i) it diminishes the terrestrial biosphere carbon storage, increasing atmospheric CO_2, but (ii) it also cools global climate due to the high ice albedo. The SST also decreases by 0.32°C at the global scale. Sea-surface temperature changes are especially pronounced in polar zones with a drop of 0.49°C in the North Atlantic and 0.47°C in the Southern Ocean) (Figure 14 compared to Figure 4b). Consequently, the ocean carbon storage increases, which lowers atmospheric CO_2. This second effect dominates and the overall result is lower atmospheric CO_2 concentration in pre-MBE simulations compared to post-MBE simulations (Figure 11). As for the other processes analysed, it only modifies atmospheric CO_2 by a few ppm, though correcting back (compared to OVC simulations) the difference pre-MBE minus post-MBE towards the observations. Nevertheless, the correlation between simulated and measured CO_2 (accounting for MIS1) is very small (-0.08) and not significant (p=0.83). The magnitude of the changes of atmospheric CO_2 among the different interglacials is once again largely underestimated as compared to observations.

Accounting for different ice sheets in the OVIC series seems to improve the model-data comparison in southern Europe for tree cover (Figure 12b) where the data are at the limit between regions of more tree coverage and less tree coverage in the model. This highlights the role of ice sheet extent in setting the vegetation pattern. Nevertheless, the uncertainty in ice sheet distribution is very large and the model-based reconstruction might not be accurate. For example, the lack of IRD (Ice Rafted Debris) from North America before MIS16 and the presence of IRD from Europe indicate that the ice sheet over Europe (Hoddell et al., 2008) could have been more extended and not the Laurentide ice sheets in North America. In addition, the

model-based reconstruction that we used shows relatively small changes of sea level equivalent between interglacials. Data reconstructions seem to indicate possible larger differences between interglacials (Spratt and Lisiecki, 2016), whose effect on the size of the land surface and the carbon cycle remains to be tested. Sensitivity experiments with prescribed idealised ice sheets designed to be very different would help to evaluate their impact.

4 Conclusions

Using a fully coupled climate model of intermediate complexity including an interactive carbon cycle, we have shown that the difference between pre-MBE and post-MBE cannot be explained by the simulated changes in ocean and vegetation induced by orbital and greenhouse gases forcing. While the oceanic response alone is in qualitative agreement with data (sign of the changes, correlation between each interglacial), it largely underestimates the amplitude of the changes. Past work suggested that either a vigorous AABW (Yin, 2013) or weak Atlantic thermohaline circulation (Köhler and Fischer, 2006) during pre-MBE interglacials could increase the oceanic carbon storage and explain the lower CO_2 than during post-MBE interglacials. Other studies for different background climates have shown opposite results with respect to the effect of ocean circulation on carbon storage. A weaker AMOC could either result in more ocean carbon storage with a pre-industrial climate (Obata, 2007; Menviel et al., 2008; Bozbiyik et al., 2011) or glacial climate (Menviel et al., 2008), or it could yield less ocean carbon storage with a pre-industrial climate (Marchal et al., 1998; Swingedouw et al., 2007b; Bouttes et al., 2012) or a glacial climate (Schmittner and Galbraith, 2008; Bouttes et al., 2012; Schmittner and Lund, 2015). Menviel et al. (2014) showed that on top of changes in NADW formation, modifications of AABW and NPDW formations could results in different oceanic carbon storage. Data indicate that the modern reduction of carbon uptake in the North Atlantic is due to a reduction in the overturning circulation (Perez et al., 2013). Because the atmospheric CO_2 change that we simulate has a low magnitude of only a few ppm, it is not yet possible to infer whether stronger or weaker overturning during pre-MBE interglacials could have significantly lowered atmospheric CO_2.

Furthermore, accounting for the vegetation response complicates the simulated response and entirely removes the qualitative agreement. The vegetation response depends on ice sheet extent and accounting for ice sheet variations limits the disagreement. Comparison of simulated vegetation changes with available pollen data indicates partial agreement, underlying the need to improve vegetation simulations and increase the data coverage to constrain more precisely the change of vegetation cover. The vegetation model in iLOVECLIM only simulates grass and trees, to better evaluate the different vegetation response to orbital and CO_2 forcings it would be useful to use a more complex terrestrial biosphere model.

We argue that additional processes need to be accounted for or should be better represented in climate models to explain the observations. It is either possible that many different processes, some of them not included in the present model, adds up to lead to the observed atmospheric CO_2 concentration, or just that a first order process is mis-represented or not included. In particular, the storage of carbon in frozen soils (permafrost) should be included in future modelling work. Response of the

Southern Ocean, the widest oceanic region with large air-sea fluxes of CO_2 is also a good candidate, given the known deficiency in coarse resolution climate models for the representation of key element of its dynamics (eddies, katabatic winds, AABW formation, brines…). The impact of ventilation changes could be tested by artificially modifying the buoyancy forcing in the areas of bottom water formation. The use of higher resolution models in this region could help to better evaluate its response to different interglacial conditions.

Acknowledgments

We are grateful to two anonymous reviewers for their useful comments. The research leading to these results has received funding from the European Union's Horizon 2020 research and innovation programme under grant agreement No 656625, project 'CHOCOLATE'. We also acknowledge WarmClim, a LEFE-INSU IMAGO project. All the simulations have been performed on avakas machine from the "Mésocentre de Calcul Intensif Aquitain (MCIA)". We thank Vincent Marieu for his assistance to set up the model on this super computer. Discussions with Anne-Sophie Kremer and Thibaut Caley were useful to mature this paper and are acknowledged.

References

Bereiter, B., Eggleston, S., Schmitt, J., Nehrbass-Ahles, C., Stocker, T. F., Fischer, H., Kipfstuhl, S., and Chappellaz, J.: Revision of the EPICA Dome C CO_2 record from 800 to 600 kyr before present, Geophys. Res. Lett., 42, 542–549, doi:10.1002/2014GL061957, 2015.

Bouttes, N., Paillard, D. and Roche, D. M.: Impact of brine-induced stratification on the glacial carbon cycle, Clim. Past, 6, 575-589, doi:10.5194/cp-6-575-2010, 2010.

Bouttes, N., Roche, D. M., and Paillard, D.: Systematic study of the impact of fresh water fluxes on the glacial carbon cycle, Clim. Past, 8, 589-607, 2012.

Bouttes, N., Roche, D. M., Mariotti, V. and Bopp, L.: Including an ocean carbon cycle model into *i*LOVECLIM (v1.0), Geosci. Model Dev., 8, 1563-1576, doi:10.5194/gmd-8-1563-2015, 2015.

Bozbiyik, A., Steinacher, M., Joos, F., Stocker, T. F., and Menviel, L.: Fingerprints of changes in the terrestrial carbon cycle in response to large reorganizations in ocean circulation, Clim. Past, 7, 319–338, doi:10.5194/cp-7-319-2011, 2011.

Brovkin, V., Ganopolski, A., Svirezhev, Y.: A continuous climate-vegetation classification for use in climate-biosphere studies, Ecological Modelling, 101 (2-3), 251-261, 1997.

Brovkin, V., Bendtsen, J., Claussen, M., Ganopolski, A., Kubatzki, C., Petoukhov, V., and Andreev, A.: Carbon cycle, vegetation and climate dynamics in the Holocene: experiments with the CLIMBER-2 model, Global Biogeochem. Cyc., 16, 1139, doi:10.1029/2001GB001662, 2002.

Calov, R., Ganopolski, A., Claussen, M., Petoukhov, V., and Greve. R.: Transient simulation of the last glacial inception, Part I: Glacial inception as a bifurcation of the climate system, Clim. Dynam., 24, 545–561, doi:10.1007/s00382-005-0007-6, 2005.

Crichton, K. A., Bouttes, N., Roche, D. M., Chappellaz, J. and Krinner, G.: Permafrost carbon as a missing link to explain CO_2 changes during the last deglaciation, Nature Geoscience, 9, 683–686, doi:10.1038/ngeo2793, 2016.

Fischer, H., Schmitt, J., Lüthi, D., Stocker, T.F., Tschumi, T., Parekh, P., Joos, F., Köhler, P., Völker, C., Gersonde, R., Barbante, C., Le Floch, M., Raynaud, D., Wolff, E.: The role of Southern Ocean processes on orbital and millennial CO_2 variations - a synthesis, Quaternary Science Reviews, 29(1-2), 193-205, doi:10.1016/j.quascirev.2009.06.007, 2010.

Ganopolski, A., Petoukhov, V., Rahmstorf, S., Brovkin, V., Claussen, M., Eliseev, A., and Kubatzki, C.: CLIMBER-2: a climate system model of intermediate complexity, Part II: Model sensitivity, Clim. Dynam., 17, 735–751, 2001.

Ganopolski, A. and Calov, R.: The role of orbital forcing, carbon dioxide and regolith in 100 kyr glacial cycles, Clim. Past, 7, 1415-1425, doi:10.5194/cp-7-1415-2011, 2011.

Goosse, H., Brovkin, V., Fichefet, T., Haarsma, R., Huybrechts, P., Jongma, J., Mouchet, A., Selten, F., Barriat, P.-Y., Campin, J.-M., Deleersnijder, E., Driesschaert, E., Goelzer, H., Janssens, I., Loutre, M.-F., Morales Maqueda, M. A., Opsteegh, T., Mathieu, P.-P., Munhoven, G., Pettersson, E. J., Renssen, H., Roche, D. M., Schaeffer, M., Tartinville, B., Timmermann, A. and Weber, S. L.: Description of the Earth system model of intermediate complexity LOVECLIM version 1.2, Geosci. Model Dev., 3, 603-633, doi:10.5194/gmd-3-603-2010, 2010.

Greve, R.: A continuum-mechanical formulation for shallow poly- thermal ice sheets, Philos. T. Roy. Soc. Lond. A, 355, 921–974, 1997.

Heuzé, C., Heywood, K. J., Stevens, D. P., and Ridley, J. K.: Southern Ocean bottom water characteristics in CMIP5 models, Geophys. Res. Lett., 40, doi:10.1002/grl.50287, 2013.

Hodell, D. A., Channell, J. E. T., Curtis, J. H., Romero, O. E., and Röhl, U.: Onset of "Hudson Strait" Heinrich events in the eastern North Atlantic at the end of the middle Pleistocene transition (~640 ka)? Paleoceanography, 23, PA4218, doi:10.1029/2008PA001591, 2008.

Köhler, P. and Fischer, H.: Simulating low frequency changes in atmospheric CO2 during the last 740 000 years, Clim. Past, 2, 57-78, 2006.

Lang, N. and Wolff, E. W.: Interglacial and glacial variability from the last 800 ka in marine, ice and terrestrial archives, Clim. Past, 7, 361-380, doi:10.5194/cp-7-361-2011, 2011.

Lisiecki, L. E., and Raymo, M. E.: A Pliocene-Pleistocene stack of 57 globally distributed benthic δ18O records, Paleoceanography, 20, PA1003, doi:10.1029/2004PA001071, 2005.

Lüthi, D., Le Floch, M., Bereiter, B., Blunier, T., Barnola, J.-M., Siegenthaler, U., Raynaud, D., Jouzel, J., Fischer, H., Kawamura, K. and Stocker, T. F.: High-resolution carbon dioxide concentration record 650,000-800,000 years before present, Nature, 453, 379-382 , doi:10.1038/nature06949, 2008.

Marchal, O., Stocker, T. F., and Joos, F.: Impact of oceanic reor- ganizations on the ocean carbon cycle and atmospheric carbon dioxide content, Paleoceanography, 13, 225–244, 1998.

Menviel, L., Timmermann, A., Mouchet, A., and Timm, O.: Meridional reorganizations of marine and terrestrial productivity during Heinrich events, Paleoceanography, 23, PA1203, doi:10.1029/2007PA001445, 2008.

Menviel, L., England, M.H., Meissner, K., Mouchet, A., Yu, J.: Atlantic-Pacific seesaw and its role in outgassing CO_2 during Heinrich events, Paleoceanography, 29, doi:10.1002/2013PA002542, 2014.

Obata, A.: Climate-Carbon Cycle Model Response to Freshwater Discharge into the North Atlantic, J. Climate, 20, 5962–5976, doi:10.1175/2007JCLI1808.1, 2007.

Oliveira, D., Desprat, S., Rodrigues, T., Naughton, F., Hodell, D., Trigo, R., Rufino, M., Lopes, C., Abrantes, F. and Sánchez Goñi, M.F.: The complexity of millennial-scale variability in southwestern Europe during MIS 11. Quaternary Research, 86(3), 373-387, doi:10.1016/j.yqres.2016.09.002, 2016.

Pérez, F. F., Mercier, H., Vázquez-Rodríguez, M., Lherminier, P., Velo, A., Pardo, P. C., Rosón, G. and Ríos, A. F.: Atlantic Ocean CO_2 uptake reduced by weakening of the meridional overturning circulation, Nature Geoscience, 6, 146–152, doi: 10.1038/NGEO1680, 2013.

Past Interglacials Working Group of PAGES: Interglacials of the last 800,000 years, Rev. Geophys., 54, 162–219, doi:10.1002/2015RG000482, 2016.

Petoukhov, V., Ganopolski, A., Brovkin, V., Claussen, M., Eliseev, A., Kubatzki, C., and Rahmstorf, S.: CLIMBER-2: A climate system model of intermediate complexity, Part I: Model description and performance for present climate, Clim. Dynam., 16, 1– 17, 2000.

Roucoux, K. H., Tzedakis, P. C., de Abreu, L., Shackleton, N. J.: Climate and vegetation changes 180,000 to 345,000 years ago recorded in a deep-sea core off Portugal, Earth and Planetary Science Letters, 249, 307-325, 2006.

Sanchez-Goni M.F., Eynaud, F., Turon, J.L., Shackleton, N.J.: High resolution palynological record off the Iberian margin: direct land-sea correlation for the Last Interglacial complex, Earth and Planetary Science Letters, 171, 123-137, 1999.

Sánchez Goñi, M.F., Rodrigues, T., Hodell, D.A., Polanco-Martinez, J.M., Alonso-Garcia, M., Hernandez-Almeida, I., Desprat, S., Ferretti, P.: Tropically-driven climate shifts in southwestern Europe during MIS 19, a low excentricity interglacial, Earth and Planetary Science Letters, 448, 81-93, 2016.

Schmittner, A. and Galbraith, E. D.: Glacial greenhouse-gas fluctuations controlled by ocean circulation changes, Nature, 456, 373–376, doi:10.1038/nature07531, 2008.

Schmittner, A., and Lund, D. C.: Early deglacial Atlantic overturning decline and its role in atmospheric CO_2 rise inferred from carbon isotopes ($\delta^{13}C$) Climate of the Past, 11, 135-152, 2015.

Spratt, R. M. and Lisiecki, L. E.: A Late Pleistocene sea level stack, Clim. Past, 12, 1079-1092, doi:10.5194/cp-12-1079-2016, 2016.

Swingedouw D., Braconnot P., Delecluse P., Guilyardi E. and Marti O.: Quantifying the AMOC feedbacks during a 2xCO2 stabilization experiment with land-ice melting, Climate Dynamics, 29, 521-534, 2007a.

Swingedouw D., Bopp L., Matras A. and Braconnot P.: Effect of land-ice melting and associated changes in the AMOC result in little overall impact on oceanic CO_2 uptake, Geophysical Research Letters 34, L23706, 2007b.

Yin, Q. Z. and Berger, A.: Insolation and CO_2 contribution to the interglacial climate before and after the Mid-Brunhes Event, Nature Geoscience, 3, 243 - 246, doi:10.1038/ngeo771, 2010.

Yin, Q. Z. and Berger, A.: Individual contribution of insolation and CO_2 to the interglacial climates of the past 800,000 years, Clim. Dynam., 38 (3-4), 709-724, 2012.

Yin, Q.: Insolation-induced mid-Brunhes transition in Southern Ocean ventilation and deep-ocean temperature, Nature, 494, 222-225, doi:10.1038/nature11790, 2013.

Captions

Figure 1: (a) Atmospheric CO_2 (ppm) record at EPICA Dome C (Luthi et al., 2008), insolation (W/m2) (b) at 65°N on 21st of June and (c) at 65°S on 21st of December, based on Berger et al. (1978).

Figure 2: Ice sheet elevation (m) in the North hemisphere simulated by the CLIMBER-2 model (Ganopolski and Calov, 2011) and used in the OVIC series for each interglacial simulation, in anomalies with respect to the pre-industrial elevation.

Figure 3: Annual SST (°C) in (a) the pre-industrial control simulation and (b-j) the interglacial simulations of the OC series with fixed vegetation and fixed ice sheets, in anomalies with respect to the pre-industrial control simulation.

Figure 4: (a, b) Annual SST difference (°C), (c, d) Meridional Overturning Circulation difference (Sv) and (e, f) Dissolved Inorganic Carbon difference (µmol/kg) between pre-MBE (MIS 13, 15, 17, 19) and post-MBE (MIS 5, 7, 9, 11) interglacials simulations for (a, c, e) the OC series with fixed vegetation and fixed ice sheets and (b, d, f) the OVC series with interactive vegetation and fixed ice sheets. The vertical black line indicates the limit between the Southern Ocean south of 32°S and the Atlantic Ocean north of 32°S. The dots on panel (a) are SST data differences based on Past Interglacials Working Group of PAGES (2016) (Table 3).

Figure 5: Meridional Overturning Circulation (Sv) in the Southern Ocean and in the Atlantic Ocean north of 32°S in (a) the pre-industrial control simulation and, (b-j) the interglacial simulations of the OC series with fixed vegetation and fixed ice sheets, in anomalies with respect to the pre-industrial control simulation. The vertical black line indicates the limit between the Southern Ocean south of 32°S and the Atlantic Ocean north of 32°S.

Figure 6: Simulated CO_2 in the interglacial simulations of the OC series as a function of the measured CO_2 from data (Luthi et al., 2008). The Pearson correlation coefficient and the p-value are indicated on top.

Figure 7: Tree cover (%) change with respect to the pre-industrial control simulation for the OVC series with interactive vegetation and fixed ice sheets.

Figure 8: Annual SST difference (°C) between simulations with interactive vegetation (OVC) and with fixed vegetation (OC).

Figure 9: Meridional Overturning Circulation difference (Sv) between simulations with interactive vegetation (OVC) and with fixed vegetation(OC). The vertical black line indicates the limit between the Southern Ocean south of 32°S and the Atlantic Ocean north of 32°S.

Figure10: Carbon stocks (GtC) in the three reservoirs (atmosphere, ocean and land) for each simulation. (a) OC series with fixed vegetation and fixed ice sheets, (b) OVC series with interactive vegetation and fixed ice sheets and (c) OVIC series with interactive vegetation and different prescribed ice sheets. The stocks are given as anomalies with respect to the control pre-industrial simulation.

Figure 11: (a) CO_2 concentration (ppm) at the end of the simulations and (b) composite (average) CO_2 (ppm) in the pre-MBE (MIS 13, 15, 17, 19) and post-MBE (MIS 5, 7, 9, 11) interglacial simulations.

Figure 12: (a, b) Tree cover (%) and (c, d) carbon storage (kgC/m^2) difference between pre-MBE (MIS 13, 15, 17, 19) and post-MBE (MIS 5, 7, 9, 11) interglacials simulations for (a, c) the OVC series with interactive vegetation and fixed ice sheets and (b, d) the OVIC series with interactive vegetation and different ice sheets. Qualitative indication of tree cover change from data are indicated with dots: blue indicates a reduction of tree cover on average during pre-MBE interglacials compared to post-MBE interglacials, and red an increase.

Figure 13: Ice sheet elevation difference (m) between the average of the pre-MBE (MIS 13, 15, 17, 19) and post-MBE (MIS 5, 7, 9, 11) interglacial simulations.

Figure 14: Annual sea surface temperature difference (°C) between the average of the pre-MBE (MIS 13, 15, 17, 19) and post-MBE (MIS 5, 7, 9, 11) interglacials with interactive vegetation and different ice sheets (OVIC). The vertical black line indicates the limit between the Southern Ocean south of 32°S and the Atlantic Ocean north of 32°S. The dots on panel (a) are SST data differences based on Past Interglacials Working Group of PAGES (2016) (Table 3).

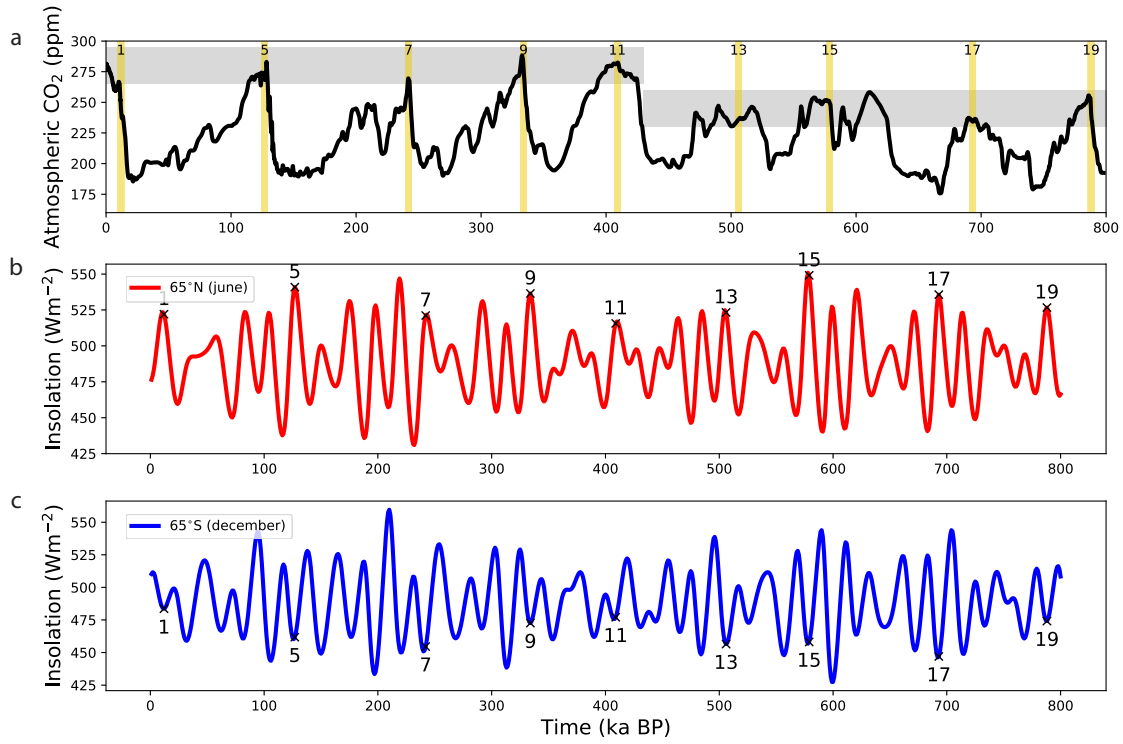

Figure 1: (a) Atmospheric CO_2 (ppm) evolution from data (Luthi et al., 2008), (b) insolation (W/m^2) (a) at 65 ° N on 21st of June and (c) at 65 ° S on 21st of December, based on Berger et al. (1978).

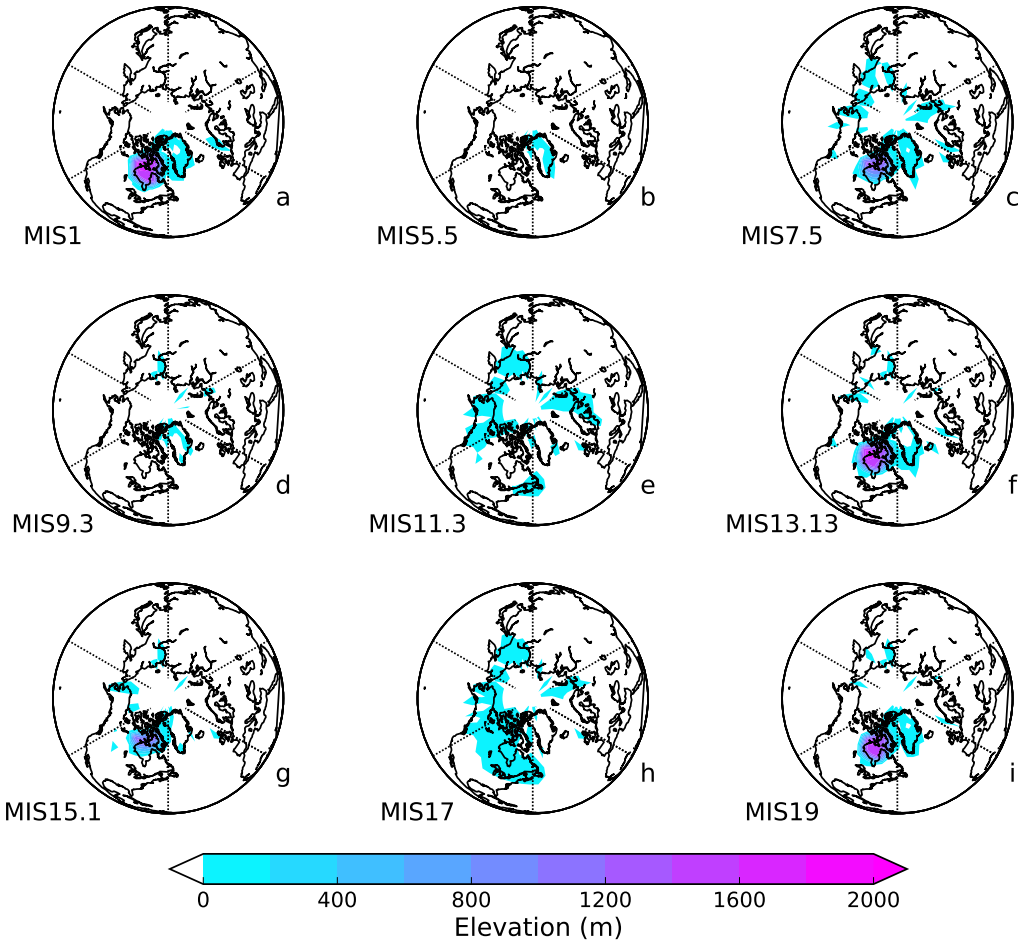

Figure 2: Ice sheet elevation (m) in the North hemisphere simulated by the CLIMBER-2 model (Ganopolski and Calov, 2011) and used in the OVIC series for each interglacial simulation, in difference with the pre-industrial elevation.

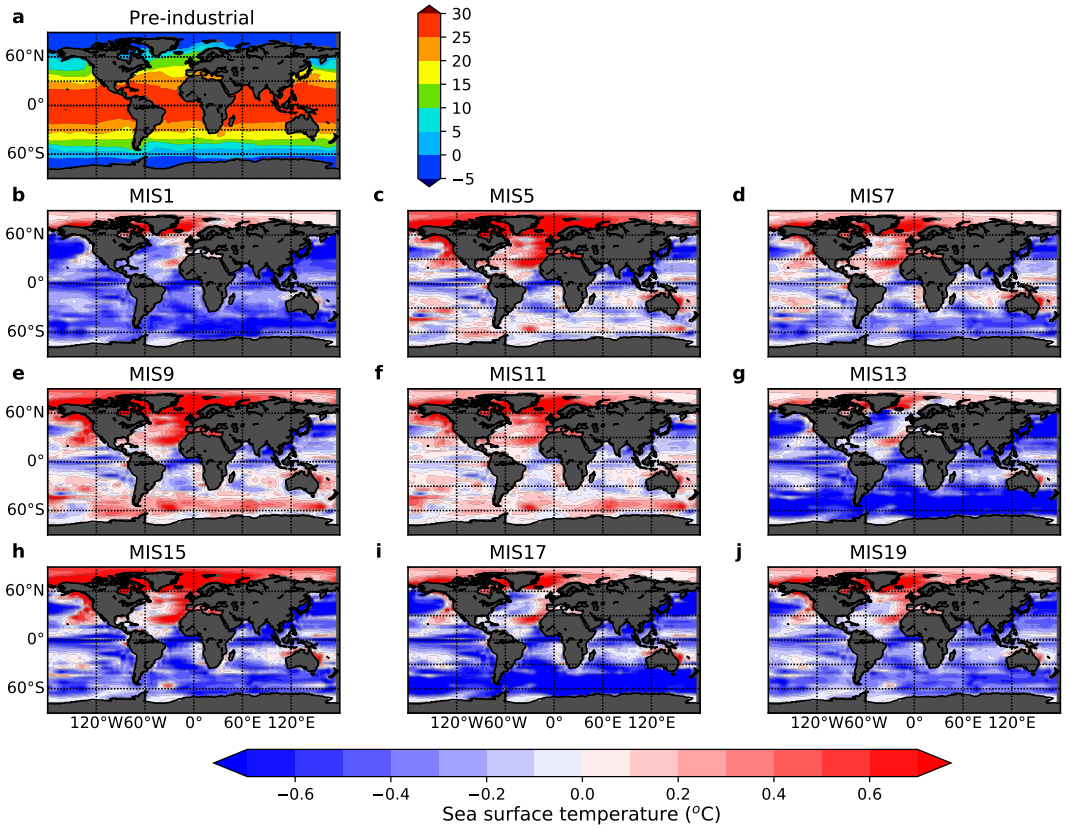

Figure 3: Annual SST ($^{\circ}$C) in (a) the pre-industrial control simulation and (b-j) the interglacial simulations of the OC series with fixed vegetation and fixed ice sheets, in anomalies with respect to the pre-industrial control simulation.

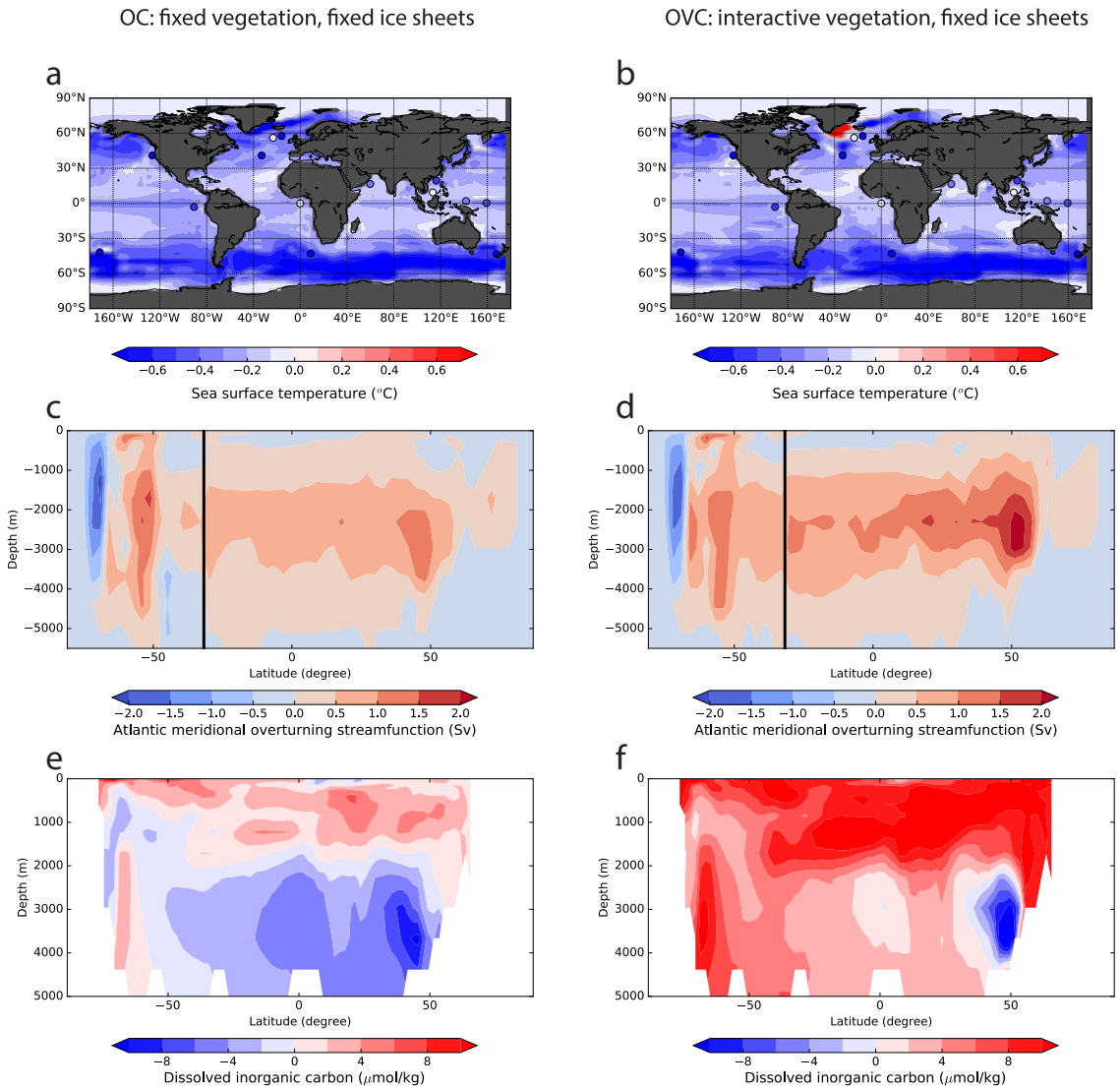

Figure 4: (a, b) Annual SST difference (˚ C), (c, d) Meridional Overturning Circulation difference (Sv) and (e, f) Dissolved Inorganic Carbon difference ($\hat{\mathrm{I}}\frac{1}{4}$mol/kg) between pre-MBE (MIS 13, 15, 17, 19) and post-MBE (MIS 5, 7, 9, 11) interglacials simulations for (a, c, e) the OC series with fixed vegetation and fixed ice sheets and (b, d, f) the OVC series with interactive vegetation and fixed ice sheets. The vertical black line indicates the limit between the Southern Ocean south of 32 ˚ S and the Atlantic Ocean north of 32 ˚ S. The dots on panel (a) are SST data differences based on Past Interglacials Working Group of PAGES (2016) (Table 3).

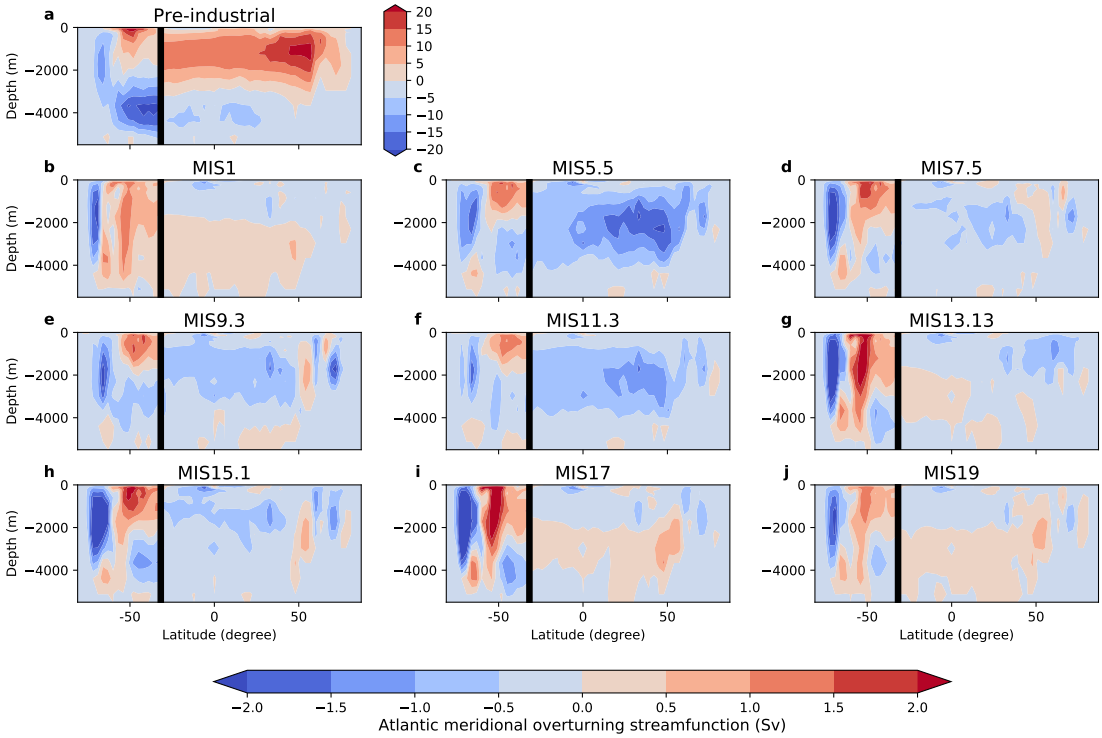

Figure 5: Meridional Overturning Circulation (Sv) in the Southern Ocean and in the Atlantic Ocean north of 32 ° S in (a) the pre-industrial control simulation and, (b-j) the interglacial simulations of the OC series with fixed vegetation and fixed ice sheets, in anomalies with respect to the pre-industrial control simulation. The vertical black line indicates the limit between the Southern Ocean south of 32 ° S and the Atlantic Ocean north of 32 ° S.

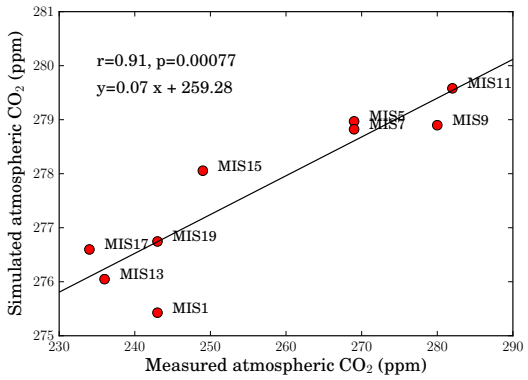

Figure 6: Simulated CO_2 in the interglacial simulations of the OC series as a function of the measured CO_2 from data (Luthi et al., 2008). The Pearson correlation coefficient and the p-value are indicated on top.

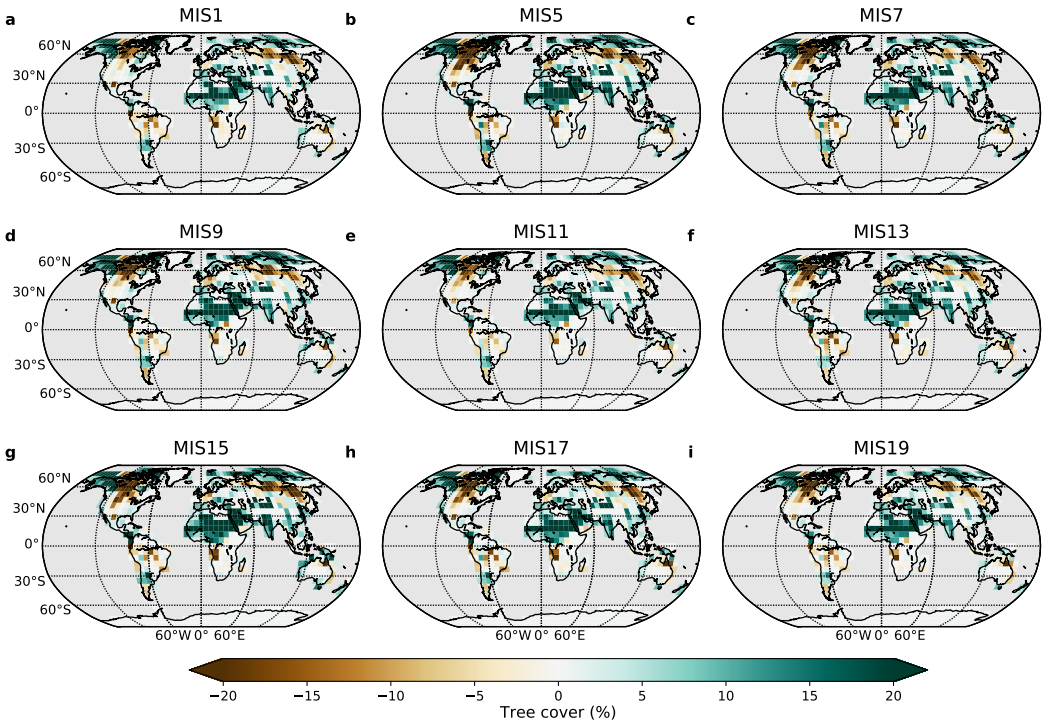

Figure 7: Tree cover (%) change with respect to the pre-industrial control simulation for the OVC series with interactive vegetation and fixed ice sheets.

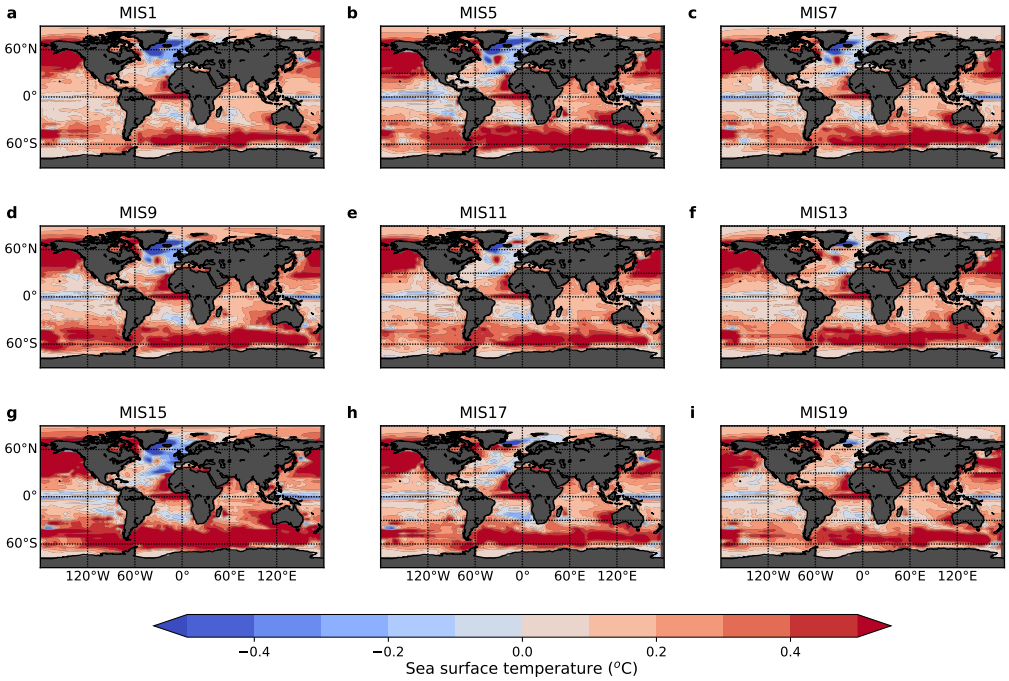

Figure 8: Annual sea surface temperature difference ($^\circ$C) between simulations with interactive vegetation (OVC) and with fixed vegetation (OC).

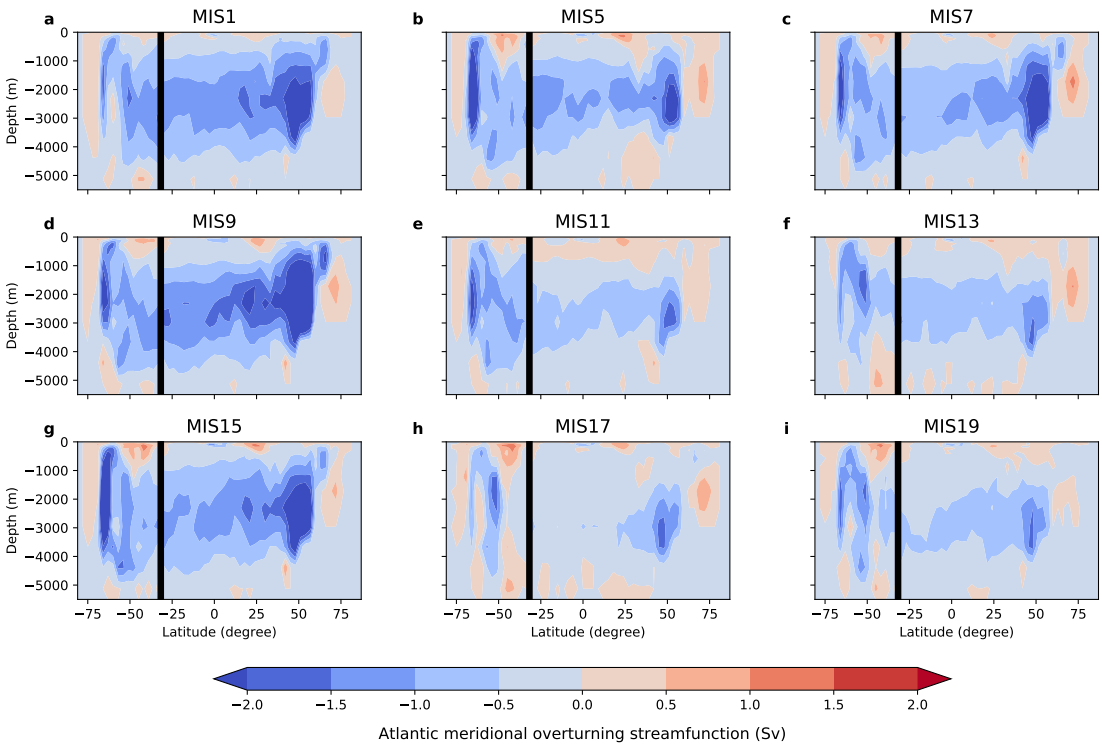

Figure 9: Meridional Overturning Circulation difference (Sv) between simulations with interactive vegetation (OVC) and with fixed vegetation(OC). The vertical black line indicates the limit between the Southern Ocean south of 32 ° S and the Atlantic Ocean north of 32 ° S.

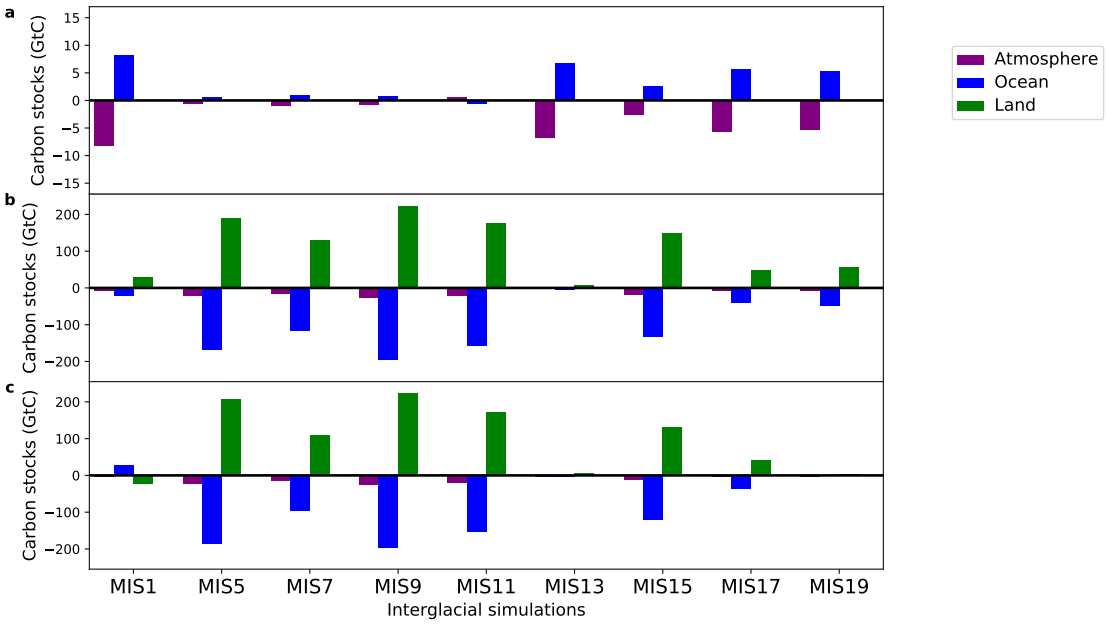

Figure10: Carbon stocks (GtC) in the three reservoirs (atmosphere, ocean and land) for each simulation. (a) OC series with fixed vegetation and fixed ice sheets, (b) OVC series with interactive vegetation and fixed ice sheets and (c) OVIC series with interactive vegetation and different prescribed ice sheets. The stocks are given as anomalies with respect to the control pre-industrial simulation.

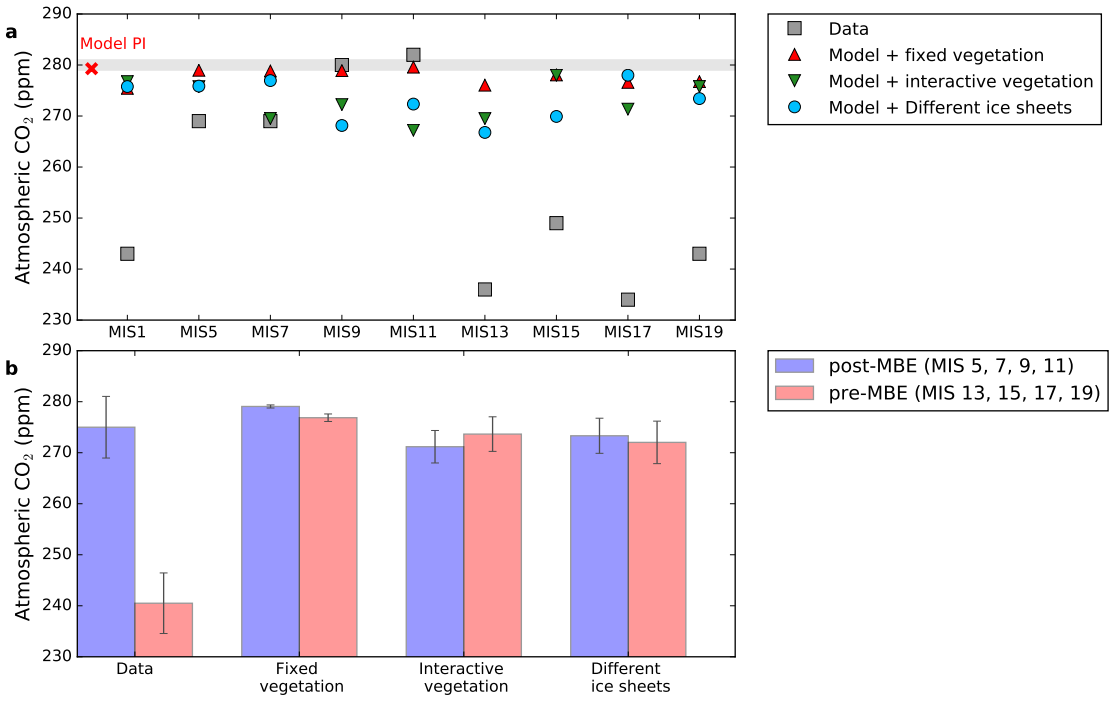

Figure 11: (a) CO_2 concentration (ppm) at the end of the simulations and (b) composite (average) CO_2 (ppm) in the pre-MBE (MIS 13, 15, 17, 19) and post-MBE (MIS 5, 7, 9, 11) interglacial simulations.

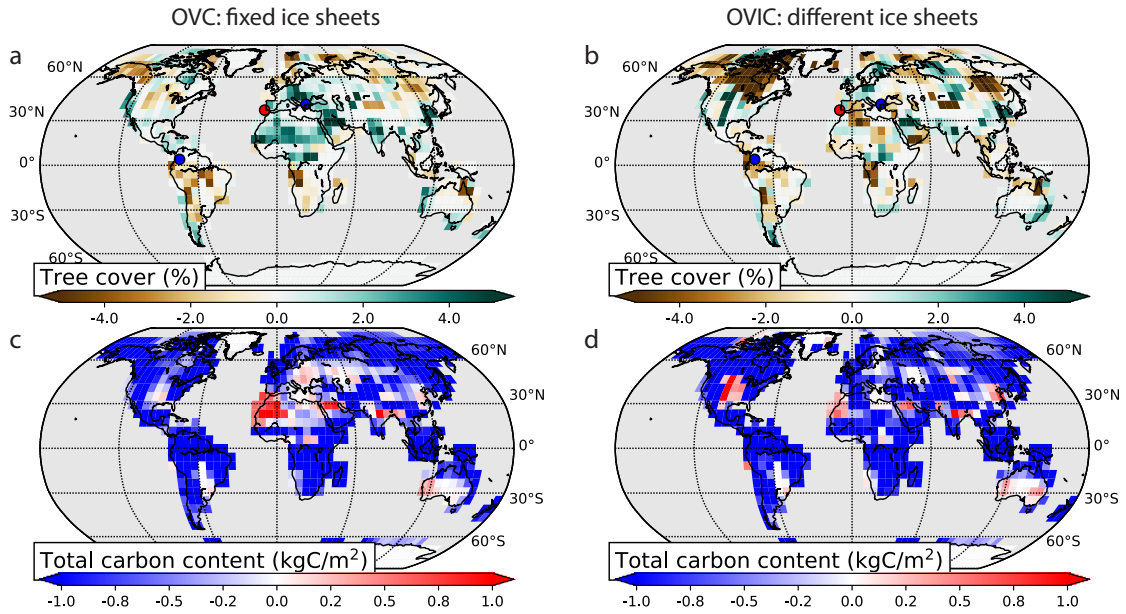

Figure 12: (a, b) Tree cover (%) and (c, d) carbon storage (kgC/m^2) difference between pre-MBE (MIS 13, 15, 17, 19) and post-MBE (MIS 5, 7, 9, 11) interglacials simulations for (a, c) the OVC series with interactive vegetation and fixed ice sheets and (b, d) the OVIC series with interactive vegetation and different ice sheets. Qualitative indication of tree cover change from data are indicated with dots: blue indicates a reduction of tree cover on average during pre-MBE interglacials compared to post-MBE interglacials, and red an increase.

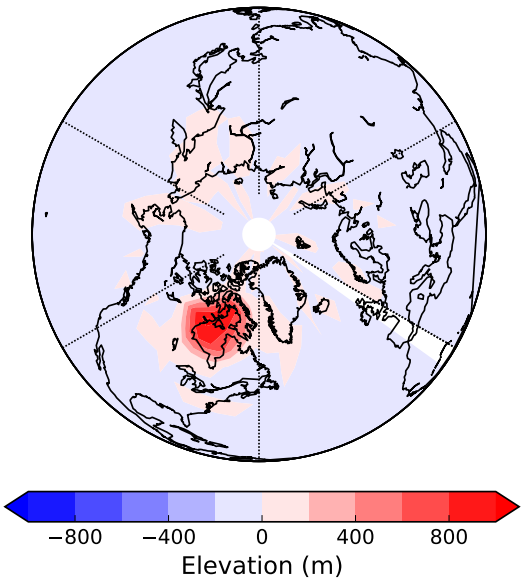

Figure 13: Ice sheet elevation difference (m) between the average of the pre-MBE (MIS 13, 15, 17, 19) and post-MBE (MIS 5, 7, 9, 11) interglacial simulations.

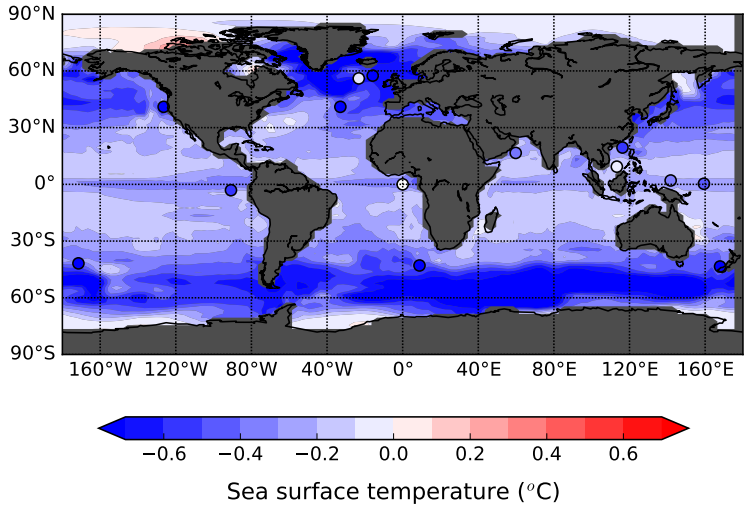

Figure 14: Annual sea surface temperature difference (˚ C) between the average of the pre-MBE (MIS 13, 15, 17, 19) and post-MBE (MIS 5, 7, 9, 11) interglacials with interactive vegetation and different ice sheets (OVIC). The vertical black line indicates the limit between the Southern Ocean south of 32 ˚ S and the Atlantic Ocean north of 32 ˚ S. The dots on panel (a) are SST data differences based on Past Interglacials Working Group of PAGES (2016) (Table 3).